Journal of Statistical Physics, Vol. 87, Nos. 1/2, 1997

Scaling of Particle Trajectories on a Lattice

Meng-She Cao[1] and E. G. D. Cohen[1]

Received June 24, 1996; final September 6, 1996

The scaling behavior of the closed trajectories of a moving particle generated by randomly placed rotators or mirrors on a square or triangular lattice is studied numerically. On both lattices, for most concentrations of the scatterers the trajectories close exponentially fast. For special critical concentrations infinitely extended trajectories can occur which exhibit a scaling behavior similar to that of the perimeters of percolation clusters. *At* criticality, in addition to the two critical exponents $\tau = 15/7$ and $d_f = 7/4$ found before, the critical exponent $\sigma = 3/7$ appears. This exponent determines structural scaling properties of closed trajectories of finite size when they approach infinity. New scaling behavior was found for the square lattice partially occupied by rotators, indicating a different universality class than that of percolation clusters. *Near* criticality, in the critical region, two scaling functions were determined numerically: $f(x)$, related to the trajectory length (S) distribution n_S, and $h(x)$, related to the trajectory size R_S (gyration radius) distribution, respectively. The scaling function $f(x)$ is in most cases found to be a symmetric double Gaussian with the same characteristic size exponent $\sigma = 0.43 \approx 3/7$ as at criticality, leading to a stretched exponential dependence of n_S on S, $n_S \sim \exp(-S^{6/7})$. However, for the rotator model on the partially occupied square lattice an alternative scaling function is found, leading to a new exponent $\sigma' = 1.6 \pm 0.3$ and a superexponential dependence of n_S on S. $h(x)$ is essentially a constant, which depends on the type of lattice and the concentration of the scatterers. The appearance of the same exponent $\sigma = 3/7$ at and near a critical point is discussed.

KEY WORDS: Lattice; particle trajectories; percolation; scaling function; criticality.

1. INTRODUCTION

In a number of previous publications[1-11] the diffusion properties of Lorentz lattice gas cellular automata has been studied. There the behavior of a point particle moving through fixed, regularly[6] or randomly[1-5, 7-11]

[1] The Rockefeller University, New York, New York 10021.

0022-4715/97/0400-0147$12.50/0

placed scatterers on the lattice sites of a variety of planar lattices has been obtained numrically. The scatterers consisted either of rotating right and left rotators or of reflecting right and left mirrors which scatter the particle either to its right or its left, respectively. The particle is constrained to move in unit time steps along the lattice bonds (of unit length) and the lattices studied were the square,[1,2,4,7] triangular,[3,7] honeycomb,[8] quasi-lattice,[8] and random lattice.[3,11] Since the scatterers are fixed on the lattice, the particle simply travels periodically on the lattice once the trajectory forms a closed orbit. In almost all cases studied so far the trajectories close exponentially fast, typically after 2^{10} time steps. However, in some cases they close power-law slowly. In that case there are extended trajectories, possibly of infinite length, which only close after a long (possibly infinite) time. Studying these extended trajectories reveals that they exhibit scaling properties, which in the case of a lattice fully occupied by scatterers, can be mapped onto a corresponding bond or site percolation problem. However, in the case of a lattice not fully occupied by scatterers, where empty sites occur and the particle trajectory can cross itself, no such mapping seems possible. Nevertheless some of the scaling properties of these trajectories are then still the same as those found for the fully occupied lattice where no such crossing can occur. The identity of the scaling properties of the closed trajectories with those of a corresponding percolation problem is exemplified, for example, by the appearance of the same two universal critical exponents that occur in the two-dimensional (bond or site) percolation problem: a fractal dimension $d_f = 7/4$ associated with the length S of the trajectories (perimeter of a percolation cluster) and the mean square distance of all points on a large trajectory of length S from the origin, R_S^2 (gyration radius squared of a percolation cluster),

$$R_S^2 \sim S^{2/d_f} \tag{1}$$

as well as the Fisher exponent $\tau = 15/7$ characterizing the probability distribution of closed trajectories (percolation clusters) of a certain length,

$$n_S \sim S^{-\tau+1} \tag{2}$$

A hyperscaling relation holds between these exponents:

$$\tau - 1 = \frac{2}{d_f} \tag{3}$$

We note that the closed particle trajectories, when mapped onto percolation clusters, are characterized here by their "surface" properties, i.e.,

their length, not, as is usually done, by their "bulk" properties, i.e., the total number of lattice sites they contain.

In this paper we introduce finer characterizations of the closed particle trajectories than by the scaling exponents τ and d_f alone. The quantities that describe the finer characterizations are: (1) The number of right and left scatterers and empty sites on a closed trajectory, i.e., N_R, N_L, and N_E, respectively; (2) the winding angle W, i.e., the number of right turns minus the number of left turns of the particle moving on a closed trajectory; and (3) the frequency with which lattice sites on the particle trajectory are visited by the moving particle. These are more detailed "structural" properties than the "gross" properties incorporated in τ and d_f. By studying these properties for finite trajectories of increasing length at criticality, we derive in this paper a number of trajectory scaling properties which include not only the asymptotic behavior for infinitely large closed trajectories, but also the approach to the asymptotic behavior. This approach is characterized by a critical size exponent σ, which also describes that of the percolation cluster perimeters at the percolation threshold.[12,13] In addition, the scaling behavior in the region near criticality, i.e., when one approaches the critical point from the outside, is obtained by the determination of two scaling functions, to be defined below, which also contain the critical size exponent σ.

The numerical algorithm we used was obtained from an efficient combination of the Ziff algorithm[13,14] (use of a virtual lattice) and a technique recently developed by Wang and Cohen[7,8] (dynamical memory allocation). The simulation was done on a virtual lattice of size 65536×65536. The lattice was divided into 1024×1024 blocks of 64×64 sites rather than 256×256 blocks of 256×256 sites as used by Ziff[13] and Wang and Cohen,[7,8] since a smaller block size is more efficient for dilute scatterer models. Sixteen bits ($2^{16} = 65536$) were used to determine the (x, y) coordinates of a site; the upper ten bits ($2^{10} = 1024$) were used for the location of the block which had been visited by the moving particle, while the lower six bits ($2^6 = 64$) were used for the site position within the block. Another array of 1024×1024 was introduced to record whether a block had been visited by the particle. The application of bit shifting, masking, etc., to look up the coordinates of blocks and sites contained in the blocks made the whole process very fast. Furthermore, the use of a dynamic memory allocation technique, where an array of pointers is generated so that each block has a corresponding pointer, allows actual memory of the states of the sites (i.e., the type of scatterer placed on the site) in the block to be assigned to its pointer only when the particle enters it (using MALLOC in C). After a trajectory is finished, only memories that had been assigned to the pointers are deleted (using FREE in C).

About 300,000 independent particles, initially placed randomly on the lattice, were studied. We only collect closed particle trajectories whose lengths are smaller than a certain limit. The trajectory is disregarded if it did not close by that number of steps. The value of the limit we used was up to 2^{21}–2^{24} time steps, depending on the concentration of the scatterers. In all the simulations there was no particle that crossed the boundary of the virtual lattice.

We have verified for the fully occupied square and triangular lattices that our calculations were made for systems of a sufficiently large number of particles and for sufficiently long times that the error bars in our figures are typically of the order of the size of the symbols. However, for the partially occupied square and triangular lattices the accuracy of our calculations decreases with the concentration of scatterers.

In order to condense the multitude of computer results we obtained, we will present the results for the rotator model on the square lattice in some detail. The results for the mirror model on the square lattice and for both models on the triangular lattice will be discussed more summarily and all results are collected in Tables I–IV. For more details we refer to ref. 15.

The organization of this paper is as follows. Section 2 deals with the behavior of the rotator model on the square lattice and discusses the closed trajectory scaling results both for a fully and a partially occupied lattice at criticality. In Section 3 the corresponding results for the mirror model are briefly summarized. In Sections 4 and 5 the critical region for the rotator and mirror models on the square lattice are discussed, respectively. In Sections 6 and 7 we discuss the closed trajectory scaling results for the triangular lattice at and near criticality, respectively, which are the same for both the rotator and the mirror model. Section 8 contains a summary of our results in four tables as well as a number of open questions.

2. CRITICAL BEHAVIOR OF THE ROTATOR MODEL ON THE SQUARE LATTICE

2.1. The Fully Occupied Lattice

In the rotator model right and left rotators are randomly placed on the sites of the lattice. A particle moves along the bonds of the lattice and its velocity is rotated either to its right or to its left by $\pi/2$ upon being scattered by a right or a left rotator, respectively. The total concentration, i.e., the fraction of the lattice occupied by scatterers C, is the sum of those of the right rotators C_R and the left rotators C_L, respectively: $C = C_R + C_L$.

For the fully occupied lattice, i.e., $C = 1$, the trajectories of the moving particle can be mapped onto the perimeters of bond percolation

clusters,[4,7,9] as was first noted by Grassberger.[16] Since the critical concentration for bond percolation on the square lattice is 1/2, the critical concentration for the rotator model is also 1/2, i.e., $C_{R_c} = C_{L_c} = 1/2$. We note that the right rotators are either on the outer side of the trajectories, in which case the trajectory is traversed clockwise, or on the inner side of the trajectories, in which case the trajectory is traversed counterclockwise (Fig. 1a). It is convenient in our numerical simulations to introduce for the analysis of the trajectories the winding angle W, which, for example, allows a determination of whether a closed trajectory is traversed clockwise or

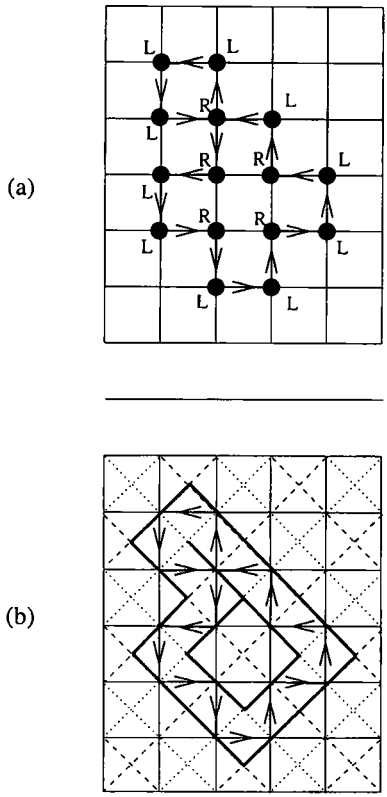

Fig. 1. (a) A typical counterclockwise closed trajectory on the square lattice. Note that all left rotators and all right rotators are on the outer side and inner side of the trajectory, respectively. Here $W = -2\pi$, $N_R = 5$, $N_L = 10$, $N_1 = 14$, $N_2 = 1$, $N = 15$, and $S = 16$. (b) The same trajectory generated by mirrors on the square lattice. Mirrors (thick solid lines) on the outer side of the trajectory form a bond percolation cluster perimeter on one of the two sublattices (dashed lines), while mirrors on the inner side of the trajectory form a bond percolation cluster perimeter on the other sublattice (dotted lines). Here $M_R = 6$ and $M_L = 9$,

counterclockwise. For a given trajectory, W is computed at each step by increasing it by $\pi/2$ if the particle is turned to the right and decreasing it by $\pi/2$ if the particle is turned to the left. Then, when the trajectory closes, the winding angle will either be 2π or -2π, corresponding to clockwise or counterclockwise rotation, respectively.

Although we expect that for large trajectories the number of right rotators N_R and the number of left rotators N_L contained in the trajectories are on average the same, there are symmetric fluctuations of N_R/N with respect to their mean value $C_{R_c} = 1/2$. The distribution of N_R/N can be fitted to a double Gaussian (Fig. 2a). The symmetry is due to the fact that the same trajectory can be generated by replacing all right (left) rotators with left (right) rotators, respectively, and reversing the particle velocity. However, if we just look at the clockwise-traversed trajectories, the fluctuations of N_R/N are no longer symmetric with respect to 1/2, since then the right rotators are always on the outer side of the trajectories, while the left rotators are always on the inner side of the trajectories. From our numerical results we found that (Fig. 3),

$$\langle N_R/N - 1/2 \rangle_c = \langle N_L/N - 1/2 \rangle_{cc} \sim N^{-0.57} \tag{4}$$

where $N = N_R + N_L$ is the total number of sites of the closed trajectory. The averages $\langle \ldots \rangle_c$ and $\langle \ldots \rangle_{cc}$ are taken over all closed trajectories containing N sites in which the particle moves clockwise (Fig. 3) and counterclockwise, respectively. There are two observations to make with regard to Eq. (4). First, the number of right and left rotators on a closed orbit become asymptotically equal, i.e., asymptotically, $N_R/N = N_L/N = 1/2$. Second, the critical exponent 0.57 is in good approximation equal to $1 - \sigma$, where the critical cluster perimeter length exponent is $\sigma = 3/7$.

It has been noticed before[4,9] that memory effects play a dominant role in the motion of the particle on the lattice with fixed scatterers and in the generation of its trajectory. However, no direct measurement of a memory effect has been given. In this paper we do so by examining how many sites on a trajectory are visited once N_1 (no memory effect) or twice N_2 (memory effect). A site on the trajectory cannot be visited more than twice on the fully occupied square lattice, since for a particle to return to the same site it has to move an even number of steps. As at each step the winding angle changes by $\pm\pi/2$, the change of the winding angle can only be either 2π or π when the particle returns to the same site, so that only N_1 and N_2 are allowed. Thus we have the sum rules

$$N_1 + N_2 = N \tag{5}$$

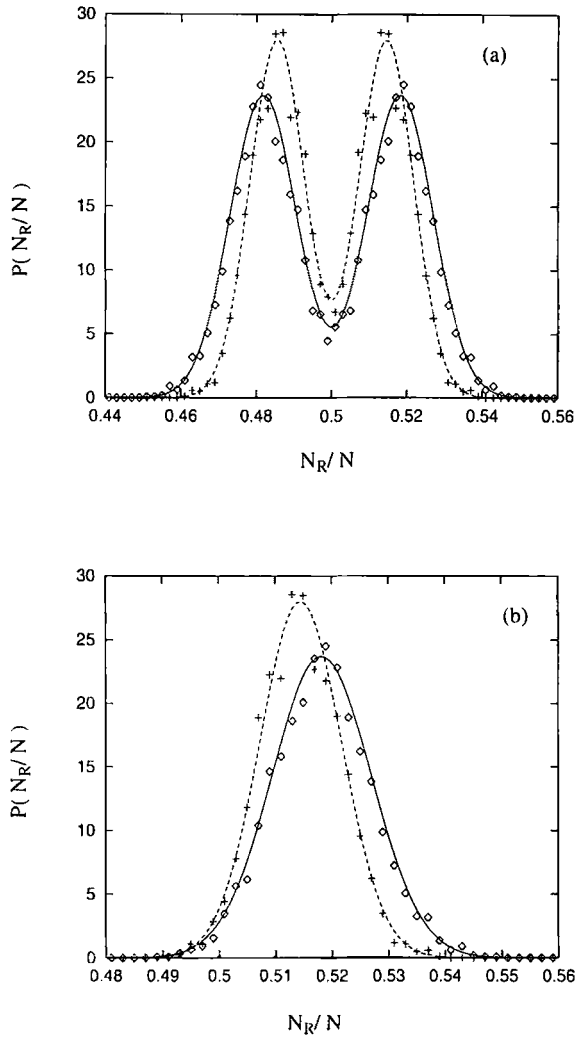

Fig. 2. The probability density $P(N_R/N)$ vs. N_R/N for the rotator model on the fully occupied square lattice. The data were obtained from trajectories consisting of 1300–1500 sites ($\diamond$) and 2000–2300 sites ($+$). (a) Both clockwise and counterclockwise trajectories are included in the data. The solid and the dashed curves are described by the double Gaussians $23.7\exp[-7058(N_R/N-0.5182)^2]+23.7\exp[-7058(N_R/N+0.5182)^2]$ and $28.0\exp[-9856(N_R/N-0.5145)^2+28.0\exp[-9856(N_R/N+0.5145)^2]$, respectively. (b) Only the clockwise trajectories are included in the data. The solid and the dashed curves are described by the Gaussians $23.7\exp[-7058(N_R/N-0.5182)^2]$ and $28.0\exp[-9856(N_R/N-0.5145)^2]$, respectively. For increasing values of N the curves become taller and narrower.

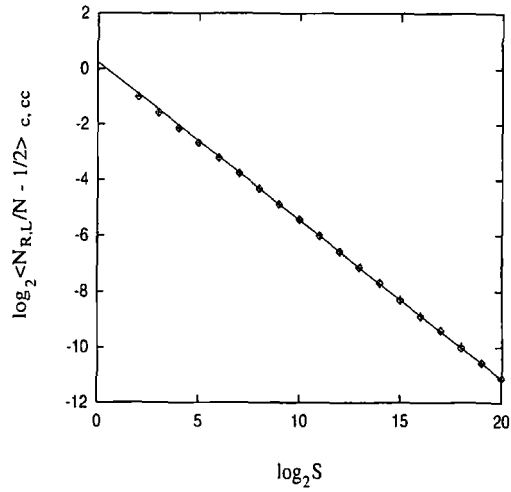

Fig. 3. Scaling behavior of N_R and N_L for clockwise (c) and counterclockwise (cc) closed trajectories, respectively, on the square lattice fully occupied by rotators, $C_R = C_L = 1/2$: $\log_2\langle N_R/N - 1/2\rangle_c$ vs. $\log_2 S$ ($\diamond$), $\log_2\langle N_L/N - 1/2\rangle_{cc}$ vs. $\log_2 S$ (+). The slope of the lines through both sets of points is -0.57.

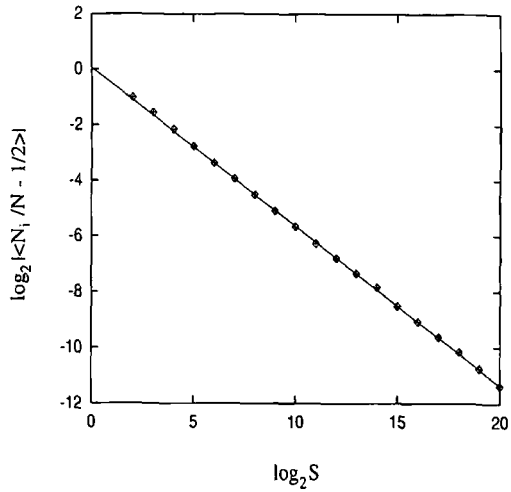

Fig. 4. Scaling behavior of N_1 and N_2 for trajectories on the square lattice fully occupied by rotators, $C_R = C_L = 1/2$: $\log_2\langle N_1/N - 1/2\rangle$ vs. $\log_2 S$ ($\diamond$). Also plotted is $\log_2\langle 1/2 - N_2/N\rangle$ vs. $\log_2 S$ (+), which has the same values. The slope of the lines through both sets of points is -0.57.

and

$$N_1 + 2N_2 = S \tag{6}$$

Our numerical results show that (Fig. 4)

$$\langle N_1/N - 1/2 \rangle = \langle 1/2 - N_2/N \rangle \sim N^{-0.57} \tag{7}$$

Note that N_1/N approaches 1/2 from above, while N_2/N approaches 1/2 from below, i.e., for infinitely large trajectories N_1/N and N_2/N are equal. The asymptotic value 1/2 for N_1/N and N_2/N was noticed independently by Ziff.[17] Furthermore, the critical exponent again appears to be related to σ.

Besides the memory effect exhibited by N_1 and N_2, there are other interesting structural properties associated with N_1 and N_2. For each site belonging to N_1 only two of four adjacent bonds belong to the trajectory, while for each site belonging to N_2 all four adjacent bonds belong to the trajectory, i.e., the site is surrounded by the trajectory. In other words, the N_1 form the "surface" of a trajectory, while the N_2 form the "bulk" of the trajectory. From Eqs. (6) and (7) it follows that

$$\langle S/N - 3/2 \rangle \sim N^{-0.57} \tag{8}$$

indicating that S and N are asymptotically proportional to each other.

2.2. The Partially Occupied Lattice

For a partially occupied lattice the trajectories can cross themselves and the outer side and inner side of the closed orbits can no longer be well defined, so that a direct mapping of the trajectories onto the perimeters of bond percolation clusters is not possible.[7,18] Nevertheless earlier numerical studies[7] still showed the existence of two critical lines symmetric with respect to the line $C_R = C_L$ and that the critical exponents τ and d_f have the same values as at $C = 1$. Moreover, we now found that the critical lines appear to be tangent to the line $C = 1$ at $C_{L_c} = C_{R_c} = 1/2$. However, the existence of these critical lines could not be established below $C = 0.56$, due to the prohibitively long numerical calculations needed.

One important consequence of the inequality of C_R and C_L at criticality for $C < 1$ is that the winding angles appear to be asymptotically proportional to the number of sites contained in the closed trajectories. As an example, we considered the critical points at concentrations $C = 0.90$, viz. $C_R = 0.477$ and $C_L = 0.423$; and $C = 0.80$, viz. $C_R = 0.44$ and $C_{L_c} = 0.36$.

We only discuss here the behavior for $C=0.90$. Then the deviation of the winding angle from its mean value $(C_{R_c}-C_{L_c})$ decays not with a power law, but with a stretched exponential law (Fig. 5),

$$\langle |W(N)/N-(C_R-C_L)| \rangle \sim 2^{-2.8\,N^{0.18}} \tag{9}$$

For N_R/N, N_L/N, and N_E/N our numerical calculations yield the following scaling relation (Fig. 6):

$$\langle |N_R/N-C_R| \rangle \sim \langle |N_L/N-C_L| \rangle \sim \langle |N_E/N-C_E| \rangle \sim N^{-0.50} \tag{10}$$

Here N_E is the number of empty sites on a trajectory and C_E the concentration of empty sites on the lattice ($C_R+C_L+C_E=1$). Note that the value of the exponent -0.50 differs from that for the fully occupied lattice -0.57, indicating that self-crossing occurs randomly as the particle generates its trajectory.

The memory effects on the partially occupied lattice are more complicated than on the fully occupied lattice. For example, the number of times that a site can be visited by the moving particle can range from one to four. We denote the number of these different types of sites by N_1, N_2, N_3, and N_4, respectively. Since each site belongs to only one of the four types N_1, N_2, N_3, or N_4, we have the following two sum rules:

$$N_1+N_2+N_3+N_4=N \tag{11}$$

$$N_1+2N_2+3N_3+4N_4=S \tag{12}$$

If the asymptotic values for N_1/N, N_2/N, N_3/N, and N_4/N are represented by K_1, K_2, K_3, and K_4, respectively, our numerical simulations show the following power-law behavior (Fig. 7):

$$\langle N_1/N-K_1 \rangle \sim \langle N_2/N-K_2 \rangle \sim \langle K_3-N_3/N \rangle \sim \langle K_4-N_4/N \rangle \sim N^{-0.39} \tag{13}$$

The sum of K_1, K_2, K_3, and K_4 is equal to one, as required by Eq. (11). We found that K_1, K_2, K_3, and K_4 are functions of the concentration C and all appear to converge, for decreasing C, to values near 1/4 (Fig. 8). The exponent -0.39 in the above equation is significantly different from the corresponding one for the fully occupied lattice, -0.57, although τ and d_f are still the same as found by Cohen and Wang.[7] The same scaling behavior is found at $C=0.80$, suggesting that this critical behavior is universal along the critical line.

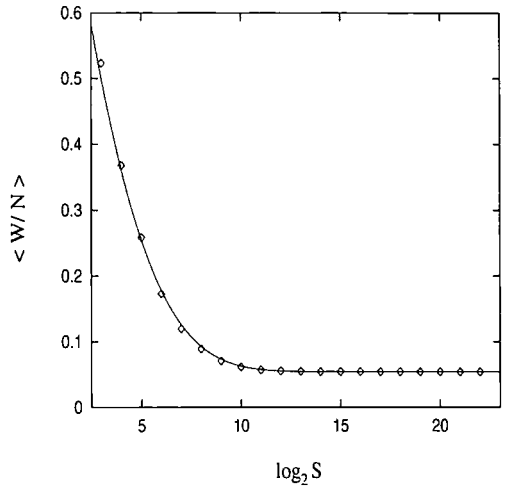

Fig. 5. Scaling behavior of the winding angle W for trajectories on the square lattice partially occupied by rotators for a typical concentration $C=0.90$ with $C_R=0.477$, $C_L=0.423$. Here $\langle |W/N-(C_R-C_L)| \rangle$ vs. $\log_2 S$ ($\diamond$) is plotted as $\langle W/N \rangle = (C_R-C_L)+7.5\times 2^{-2.80\,S^{0.18}}$ (solid curve) vs. $\log_2 S$, since all $W/N > (C_R-C_L)$.

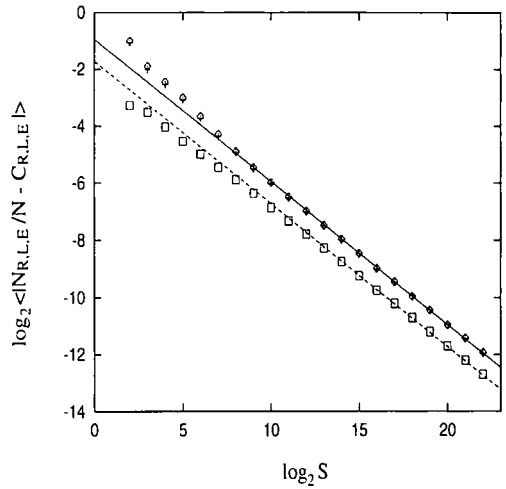

Fig. 6. Scaling behavior of N_R, N_L, and N_E for trajectories on the square lattice partially occupied by rotators for $C=0.90$ with $C_R=0.477$, $C_L=0.423$, $C_E=0.10$: $\log_2\langle |N_R/N-C_R| \rangle$ vs. $\log_2 S$ ($\diamond$), $\log_2\langle |N_L/N-C_L| \rangle$ vs. $\log_2 S$ ($+$), $\log_2\langle |N_E/N-C_E| \rangle$ vs. $\log_2 S$ ($\square$). The slope of the lines through the points is -0.50.

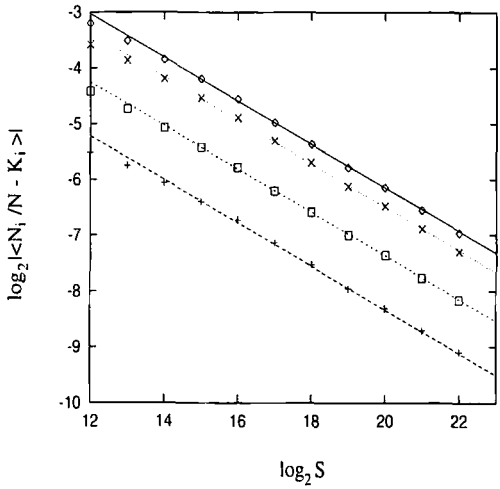

Fig. 7. Scaling behavior of N_1, N_2, N_3, and N_4 for trajectories on the square lattice partially occupied by rotators for $C=0.90$ with $C_R=0.477$, $C_L=0.423$, $C_E=0.10$: $\log_2\langle N_1/N-K_1\rangle$ vs. $\log_2 S$ ($\diamond$), $\log_2\langle N_2/N-K_2\rangle$ vs. $\log_2 S$ (+), $\log_2\langle K_3-N_3/N\rangle$ vs. $\log_2 S$ ($\square$), $\log_2\langle K_4-N_4/N\rangle$ vs. $\log_2 S$ ($\times$), where the values of K_1, K_2, K_3, and K_4 are 0.3047, 0.2671, 0.2223, and 0.2056, respectively. The slope of the lines through the points is -0.39.

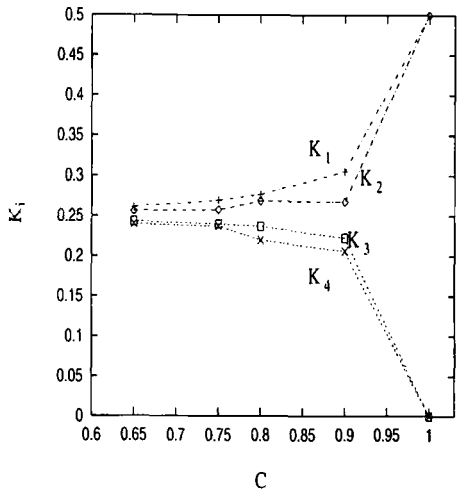

Fig. 8. Values of K_1 ($\diamond$), K_2 (+), K_3 ($\square$), and K_4 ($\times$) for trajectories on the square lattice partially occupied by rotators as a function of C. The lines through the points are drawn to guide the eye.

From Eqs. (12) and (13) it follows that,

$$\langle S/N - 2.3670 \rangle \sim N^{-0.39} \tag{14}$$

Here the constant -2.3670 for $C = 0.8$ is close to the apparent asymptotic value $S/N = 2.5$ derived from Eqs. (12) and (13), assuming the K_i all approach 0.25 for $C \to 0$.

We note that the sites that belong to N_2 can be separated into two classes: those that only have three adjacent bonds traversed by the particle and those that have four adjacent bonds traversed by the particle, respectively. The former together with N_1 form the "surface" of the trajectories, while the latter together with N_3 and N_4 form the "bulk" of the trajectories.

3. CRITICAL BEHAVIOR OF THE MIRROR MODEL ON THE SQUARE LATTICE

3.1. The Fully Occupied Lattice

In the mirror model the scatterers consist of right mirrors (tilted to the right by $\pi/4$) and left mirrors (tilted to the left by $\pi/4$), which reflect the particle upon collision like a photon is reflected from a mirror (Fig. 1b). C_R and C_L are now the concentrations of right mirrors and left mirrors, respectively, and $C = C_L + C_R$. It has been shown[4,7,19] that $C = 1$ is a critical line for the mirror model. Only for $C_{R_c} = C_{L_c} = 1/2$ can the mirror model and the rotator model be mapped onto each other. That is, by properly replacing right mirrors and left mirrors by either left rotators or right rotators we can produce the same trajectory with the same probability. For $C_R \neq C_L$ the trajectories of the two models can still be mapped onto each other, but the probability to generate the same trajectory by mirrors is no longer the same as by rotators, so that these two models can no longer be mapped onto each other.

The mirror model can, for all $C = 1$, still be mapped onto an isotropic bond percolation problem at criticality. Therefore the trajectory length distribution, characterized by $\tau = 15/7$, and the fractal dimension $d_f = 7/4$ are still the same as before. However, σ can no longer be defined for the mirror model at $C = 1$, because we are on a critical line rather than at a critical point, as was the case for the rotator model.

Unlike in the rotator model, in the mirror model right mirrors can either be on the outer side or on the inner side of a trajectory (Fig. 1b). Therefore the method of separating trajectories into clockwise and counterclockwise ones will not break the symmetry between the number of right mirrors M_R and the number of left mirrors M_L on the trajectories. Indeed,

our numerical results show that the distribution of M_R/N ($N = M_R + M_L$) is a Gaussian centered at C_R rather than a double Gaussian as we found in the rotator model (Fig. 2b). The following power-law describes how this distribution narrows as N increases:

$$\langle |M_R/N - C_R| \rangle = \langle |M_L/N - C_L| \rangle \sim N^{-0.50} \tag{15}$$

The exponent 0.50 is due to the fact that $C = 1$ is a critical line: One cannot tell then at which concentration a large trajectory is generated, so that the number M_R/N can fluctuate freely around its mean value C_R.

Memory effects can be studied in the same way as for the rotator model, because each site on the trajectories can only be visited either once or twice, the same as for the fully occupied rotator model. Our numerical results show that the scaling behavior of N_1/N and N_2/N is the same as that for the rotator model, except that the asymptotic value now depends on the concentration C_R,

$$\langle N_1/N - a(C_R) \rangle = \langle b(C_R) - N_2/N \rangle \sim N^{-0.57} \tag{16}$$

From $N_1 + N_2 = N$ we have $a(C_R) + b(C_R) = 1$. For $C_R > 1/2$ our simulations show that $a(C_R)$ is monotonically decreasing with C_R, while for $C_R < 1/2$, $a(C_R)$ is monotonically increasing with C_R (Fig. 9). At $C_R = C_L = 1/2$ we recover the result of the rotator model, i.e., $a(1/2) = b(1/2) = 1/2$.

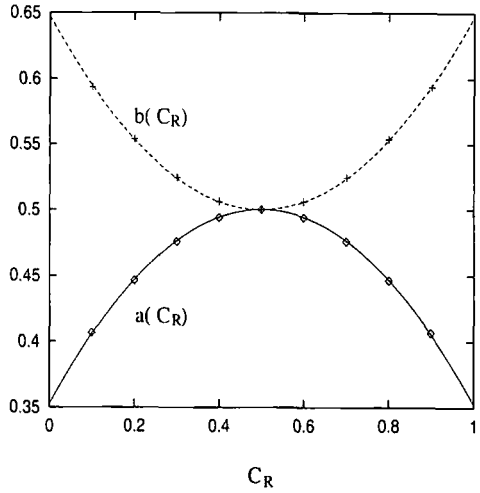

Fig. 9. Plots of $a(C_R)$ vs. C_R ($\diamond$) and $b(C_R)$ vs. C_R ($+$) for the mirror model on the fully occupied square lattice. The solid and the dashed lines are described by $0.50 + 0.59(0.25 - C_R C_L)$ and $0.50 - 0.59(0.25 - C_R C_L)$, respectively.

The scaling behavior for S/N can be derived from the relation $N_1 + 2N_2 = S$ and Eq. (16),

$$\langle S/N - [1 + b(C_R)] \rangle \sim N^{-0.57} \tag{17}$$

This scaling behavior is the same as that found for the fully occupied rotator model, Eq. (8), except that the asymptotic value is now a function of C_R rather than a single value 3/2 as for the rotator model.

3.2. The Partially Occupied Lattice

Here we only give a very brief discussion of the mirror model on a partially occupied square lattice. Again, this model cannot be mapped onto a percolation model due to the fact that trajectories can cross themselves. Previous studies have shown that the distribution of the size of closed trajectories and the fractal dimension of large trajectories are drastically changed as soon as $C < 1$: $\tau = 1$ and $d_f = 2$, with logarithmic corrections,[4,7,20,21] indicating a first-order phase transition. It has also been shown by numerical simulations that the moving particle exhibits superdiffusive behavior.[7,21]

4. CRITICAL REGION OF THE ROTATOR MODEL ON THE SQUARE LATTICE

4.1. The Fully Occupied Lattice

In the critical region *near* criticality, i.e., for the critical behavior when the critical point is approached from the outside, in addition to the scaling exponents τ, d_f, and σ, which already appeared in the previous section, one needs a scaling function, defined by[12]

$$n_S = S^{-\tau+1} f[(C_R - C_{R_c})\, S^{\sigma}] \tag{18}$$

where n_S is the probability to find a closed trajectory of length S and C_{R_c} the critical concentration of right rotators on the lattice. The scaling function $f(x)$ yields more detailed information about the trajectory length distribution than the exponent σ, where $x = (C_R - C_{R_c})\, S^{\sigma}$. Since there are no infinitely extended trajectories away from criticality, $f(x)$ must vanish when $x \to \infty$. The exponent $-\tau + 1$ instead of the usual τ occurs because the trajectories are constructed here from what corresponds in percolation theory to a seed and the number of choices to put the seed on a trajectory is proportional to the size of the trajectory itself.[13] Note that since

$x=(C_R-C_{R_c})\,S^\sigma$, in order to make $f(x)$ invariant, i.e., concentration independent, we need to give C_{R_c} and σ each a unique value. This provides an alternative method to compute both the critical exponent σ and the critical concentration C_{R_c} from numerical data obtained at a few different concentrations in the critical region.

In addition to $f(x)$ we considered a scaling function $h(x)$ introduced by Stauffer and Aharony[12]

$$R_S=S^{1/d_f}h[(C_R-C_{R_c})\,S^\sigma] \tag{19}$$

where R_S is the gyration radius of a closed trajectory of length S. The scaling function $h(x)$ characterizes corrections to the fractal dimension as one moves away from criticality. From our numerical simulations we found, however, that $h(x)$ is essentially a constant for all x. This implies that $R_S\sim S^{1/d_f}$ holds quite accurately in practice even for small trajectories, i.e., away from criticality.

Previous numerical determinations of the exponent σ were based on the calculation of the first moment of the trajectory length distribution[13,14,18,22] $\langle S\rangle$, which is divergent at criticality,

$$\begin{aligned}\langle S\rangle &=\sum_S^\infty Sn_S=\sum_S^\infty S^{-\tau+2}f((C_R-C_{R_c})\,S^\sigma)\\ &\sim(C_R-C_{R_c})^{-(3-\tau)/\sigma}\end{aligned} \tag{20}$$

Since $\langle S\rangle\sim(C_R-C_{R_c})^{-\gamma}$ by definition, one has for the critical exponent $\gamma=(3-\tau)/\sigma=2$. In this paper we also compute the average of the mean square displacement of all trajectories $\langle R^2\rangle$, which also diverges at criticality,

$$\begin{aligned}\langle R^2\rangle &=\sum_S^\infty R_S^2 n_S\\ &=\sum_S^\infty S^{-\tau+1+2/d_f}f((C_R-C_{R_c})\,S^\sigma)\,h^2((C_R-C_{R_c})\,S^\sigma)\\ &\sim(C_R-C_{R_c})^{-(2+2/d_f-\tau)/\sigma}\end{aligned} \tag{21}$$

If we define a critical exponent ρ by $\langle R^2\rangle\sim(C_R-C_{R_c})^{-\rho}$, we have $\rho=(2+2/d_f-\tau)/\sigma=7/3=2.333$. This hyperscaling relation is independent of the specific form of $f(x)$ and $h(x)$. Note that the upper limit of the summations in Eqs. (20) and (1) is infinity, which poses a difficulty when getting very close to the critical point, since the dominant closed trajectories are

then too large to generate on the computer. On the other hand, we can still compute the scaling functions $f(x)$ and $h(x)$ by making a large cutoff (2^{24}) in S, so that trajectories whose length is bigger than 2^{24} are not considered. Although then the tail of $f(x)$ will be truncated by the cutoff, the remaining part still yields sufficient information to determine σ. The calculation of each of the scaling functions $f(x)$ or $h(x)$ as well as that of $\langle S \rangle$ or $\langle R^2 \rangle$ at each concentration were carried out this way and involved 500,000 and 30,000 particle trajectories, respectively.

The scaling function $f(x)$ can be computed directly from Eq. (18), using the known values of the exponents σ and τ and the critical concentration C_{R_c},

$$f\left(\left(C_R - \frac{1}{2}\right) S^{\sigma}\right) = \frac{n_S}{S^{-\tau+1}} = S^{8/7} n_S \tag{22}$$

Note that since n_S is the probability to find a trajectory of length S, the right-hand side of Eq. (22) is an average of $S^{8/7}$ taken over trajectories of length S and can be easily determined in our numerical simulations. Also, $f(x)$ must be symmetric with respect to $x=0$, since the probability to generate the same trajectory is invariant under the transformation of interchanging C_R and C_L.

Our numerical calculations of the scaling function $f(x)$ were carried out at $C_R = 0.47$, 0.48, and 0.49, respectively. We found that the scaling functions obtained at these three concentrations collapse into a single curve, which could be fitted to a double Gaussian, i.e., a sum of two overlapping Gaussians (Fig. 10),

$$f(x) = 1.03e^{-2.25(x+0.86)^2} + 1.03e^{-2.25(x-0.86)^2} \tag{23}$$

Note that we determined 60 values of $f(x)$ for each C_R, so that the curve in Fig. 10 contains 180 points. When $x \gg 1$, $f(x)$ can be approximated by

$$f(x) \sim e^{-2.25x^2} \tag{24}$$

Therefore, n_S exhibits a stretched exponential decay for large S: $n_S \sim e^{-S^{6/7}}$, in contrast to the exponential decay reported in the literature[18,22] based on the solution of the percolation problem on the Bethe lattice.

In order to calculate $h(x)$, we first computed the product of $h(x) f(x)$. From Eqs. (18) and (19) we have

$$h(C_R - C_{R_c}) f(C_R - C_{R_c}) = n_S \frac{R_S}{S^{\tau - 1 + d_f}} \tag{25}$$

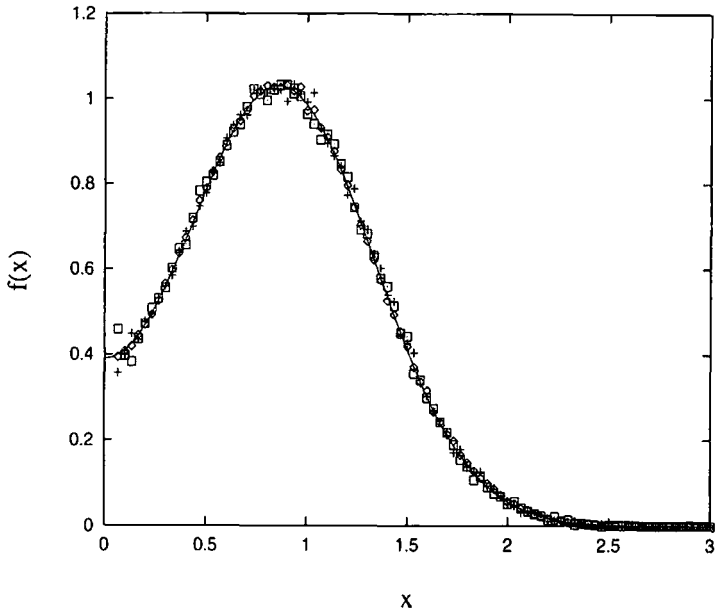

Fig. 10. The scaling function $f(x)$ vs. x for the rotator model on a fully occupied square lattice computed at $C = C_{R_c} + 0.01$ ($\diamond$), $C = C_{R_c} + 0.02$ ($+$), and $C = C_{R_c} + 0.03$ ($\square$). The curve is described by a double Gaussian $f(x) = 1.03 \exp[-2.25(x+0.86)^2] + 1.03 \exp[-2.25(x-0.86)^2]$. The deviations between $f(x)$ and the numerical data near $x = 0$ in this and later similar figures are due to the failure of scaling for small trajectories.

The right-hand side of Eq. (25) is just the average of $R_S/S^{\tau-1+d_f}$ for fixed S, which can be easily calculated numerically. Our numerical results show then that $h(x) f(x)$ is proportional to $f(x)$, Eq. (23) (Fig. 11),

$$f(x)\, h(x) = 0.39e^{-2.25(x+0.86)^2} + 0.39e^{-2.25(x-0.86)^2} \tag{26}$$

so that $h(x)$ is essentially a constant, 0.37.

We have also obtained the first moment of the trajectory length distribution as a function of $C_R - C_{R_c}$. Our numerical calculations show the power-law behavior

$$\langle S \rangle = (C_R - C_{R_c})^{-\gamma} \tag{27}$$

where $\gamma = 2.00 \pm 0.01$ (Fig. 12), in good agreement with the exact result $\gamma = (3-\tau)/\sigma = 2$. Our numerical results for the mean square displacement of the trajectories also show a power-law behavior,

$$\langle R^2 \rangle \sim (C_R - C_{R_c})^{-\rho} \tag{28}$$

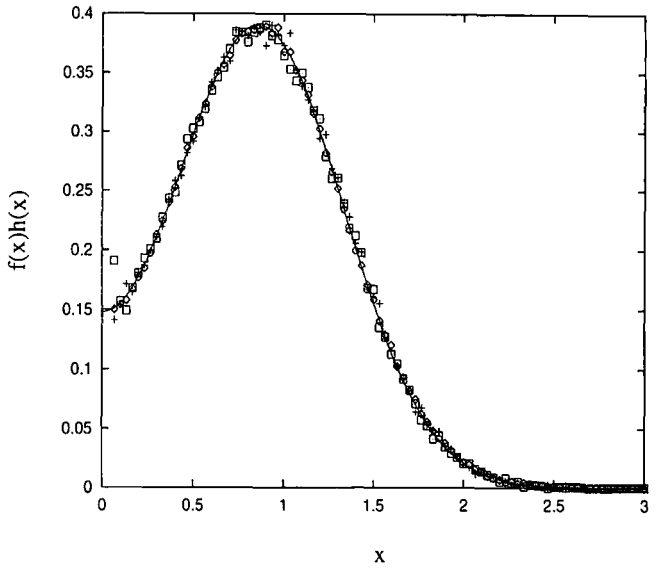

Fig. 11. The scaling function $f(x)\,h(x)$ vs. x for the rotator model on a fully occupied square lattice computed at $C = C_{R_c} + 0.01$ ($\diamond$), $C = C_{R_c} + 0.02$ ($+$), and $C = C_{R_c} + 0.03$ ($\square$). The curve is described by a double Gaussian $f(x)\,h(x) = 0.39\ \exp[-2.25(x+0.86)^2] + 0.39\ \exp[-2.25(x-0.86)^2]$.

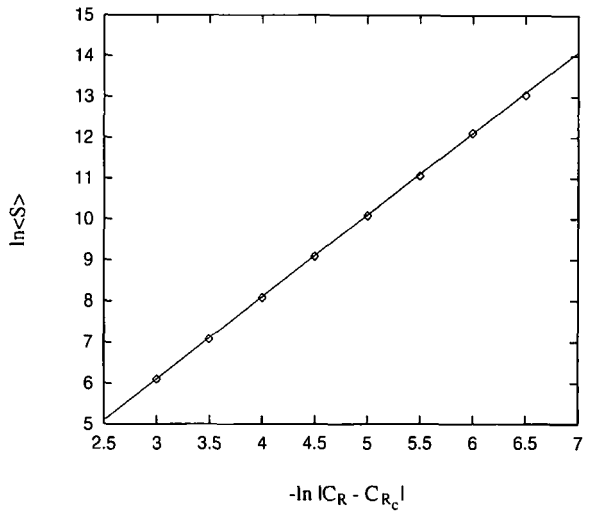

Fig. 12. Plot of $\ln\langle S\rangle$ vs. $-\ln|C_R - C_{R_c}|$ for the rotator model on the fully occupied square lattice. The slope of the fitting line is 2.00.

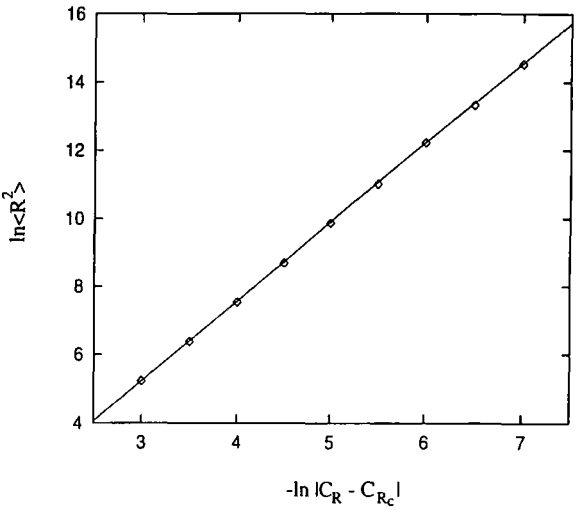

Fig. 13. Plot of $\ln\langle R^2\rangle$ vs. $-\ln|C_R - C_{R_c}|$ for the rotator model on the fully occupied square lattice. The slope of the fitting line is 2.33.

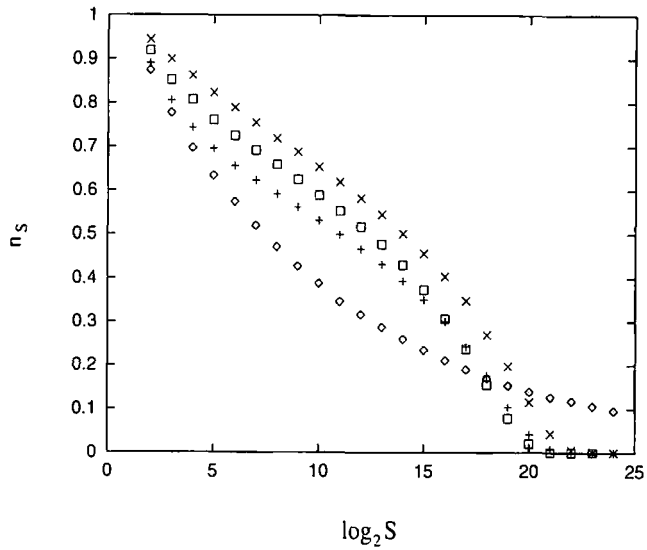

Fig. 14. Plot of n_S vs. S for the rotator model on the square lattice at concentrations $C_R = C_L = 0.50$ ($\diamond$), $C_R = C_L = 0.485$ ($+$), $C_R = C_L = 0.45$ ($\square$), and $C_R = C_L = 0.40$ ($\times$). Particle trajectories close very slowly near criticality: on line $C_R = C_L$, fastest for $C_R = C_L = 0.45$, after 2^{21} time steps.

where $\rho = 2.33 \pm 0.01$ (Fig. 13), in good agreement with the exact result $\rho = (2 + 2/d_f - \tau)/\sigma = 1/\sigma = 7/3 = 2.333$.

As a check, we also used a different method, the so-called histogram method, to calculate the scaling function $f(x)$ for different concentrations from data computed at a given initial concentration C_R.[15] A similar method has been used by Leath[23] to study the scaling behavior of percolation clusters and by Ferrenberg and Swendsen[24] to study the critical behavior of the Ising model. The initial data that we used were computed at the concentration $C_R = 0.51$. From these we generated the scaling functions $f(x)$ for $C_R = 0.52$, 0.53, 0.54, 0.55, all of which fell on the same curve. Thus this method gives results consistent with those of the first one. These results also show that the critical region in concentration is at least as large as 0.05.

4.2. The Partially Occupied Lattice

For $C < 1$ the particle trajectories can no longer be mapped onto a percolation problem, because the trajectories can cross themselves. We

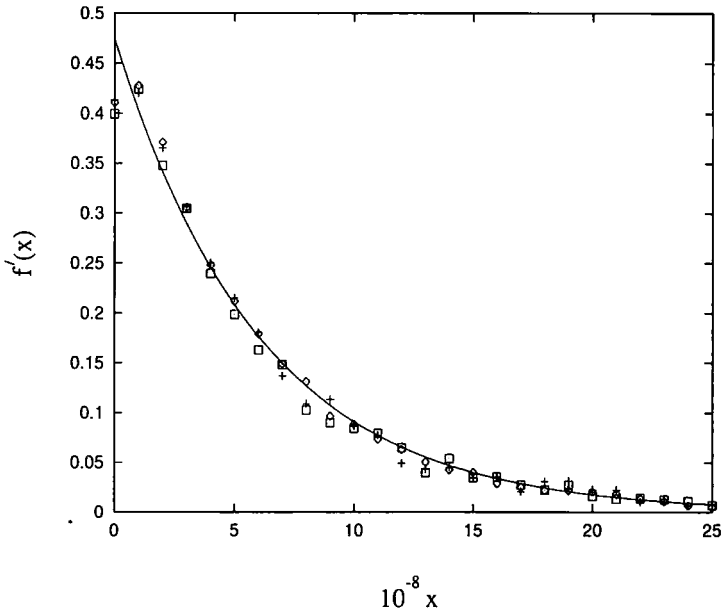

Fig. 15. The scaling function $f'(x)$ vs. x for the rotator model on the partially occupied square lattice computed at $C = C_{R_c} + 0.02$ ($\diamond$), $C = C_{R_c} + 0.015$ ($+$), and $C = C_{R_c} + 0.01$ ($\square$). The curve is described by an exponential function $f'(x) = 0.475 \exp(-0.165 \times 10^{-8} x)$.

found numerically that in addition to the exponent σ occurring in the previous section, they are also characterized by a different exponent σ', suggesting a new scaling behavior.

The simplest way to study the critical behavior near criticality for $C<1$ is to approach the critical point $C_{R_c}=C_{L_c}=1/2$ along the line $C_R=C_L$, which is perpendicular to the critical line at $C_R=C_L=1/2$. Assuming that the cluster size distribution has a form similar to Eq. (18), we set (cf. Fig. 14):

$$n_S=S^{-\tau+1}f'((1-C)S^{\sigma'}) \tag{29}$$

where $f'(x)$ is a new scaling function, with x defined as $(1-C)S^{\sigma'}$. Since x cannot be negative, $f'(x)$ must be asymmetric with respect to $x=0$, in contrast to $f(x)$ of Eq. (23). The exponent τ, however, must be the same as before, since for $C=1$ the previously established relation $n_S\sim S^{-\tau+1}$ must be recovered.

The computation of the new scaling function $f'(x)$ is much more time-consuming than that for the fully occupied lattice, but we can still compute it by making a cutoff, i.e., trajectories whose length are bigger than a fixed

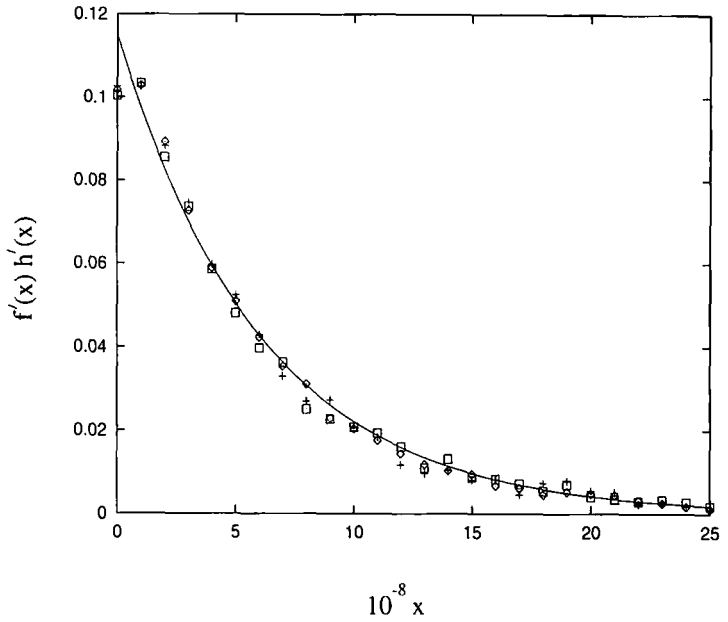

Fig. 16. The scaling function $f'(x)\,h'(x)$ vs. x for the rotator model on the partially occupied square lattice computed at $C=C_{R_c}+0.02$ ($\diamond$), $C=C_{R_c}+0.015$ ($+$), and $C=C_{R_c}+0.01$ ($\square$). The curve is described by an exponential function $f'(x)\,h'(x)=0.115\exp(-0.165\times10^{-8}x)$.

number are disregarded. In our simulations, we took this cutoff at 16 million time steps. By choosing $\sigma' = 1.6$, we find that the scaling functions obtained for different concentrations $C = 0.99$, 0.985, 0.98 all collapse to a single curve (Fig. 15),

$$f'(x) = 0.475e^{-(1.65 \times 10^{-8}x)} \tag{30}$$

where for each C, 25 points have been computed, so that curve in Fig. 15 contains 75 points. Note that since $x \sim S^{1.6}$, $f'(x)$ decays as a super-exponential function of S, $n_S \sim e^{-S^{1.6}}$. In fact, Eq. (30) obtains for values of $\sigma' = 1.6 \pm 0.3$. This large value of σ' as compared to $\sigma = 3/7$ indicates that the typical size of closed trajectories upon approach to criticality increases much slower to infinity along the line $C_R = C_L$ than along the line $C_R + C_L = 1$.

The other scaling function $h'(x)$ is obtained from the calculation of $f'(x)\,h'(x)$, which we found again to be proportional to $f'(x)$ (Fig. 16),

$$f'(x)\,h'(x) = 0.115e^{-(1.65 \times 10^{-8}x)} \tag{31}$$

so that $h'(x) = 0.115/0.475 = 0.24$ independent of x. The exponents γ' and ρ' can be obtained from $\gamma' = (3-\tau)/\sigma' = 0.54$ and $\rho' = (2 + 2/d_f - \tau)/\sigma' = 0.63$, respectively, and are both much smaller than those for $C = 1$.

5. CRITICAL REGION OF THE MIRROR MODEL ON THE SQUARE LATTICE

It has been shown by mapping the mirror model to a percolation problem that $C = 1$ is a critical line,[4,7,17] i.e., the length distribution and the fractal dimension of the trajectories have the same power-law behavior as for the corresponding percolation problem at criticality, $n_S \sim S^{-\tau+1} \sim S^{-8/7}$, so that $\tau = 15/7$ and $d_f = 7/4$, respectively. However, the average trajectory size $\langle S \rangle$ and the mean square displacement $\langle R^2 \rangle$ are both divergent along the critical line, so that the exponent σ does not appear here.

For $C \lesssim 1$ the mirror model can no longer be mapped onto a percolation problem. It was found numerically that the critical exponents are drastically changed from those at $C = 1$; $n_S \sim (\ln S)^{-1}$ and $d_f = 2$ with logarithmic corrections.[4,7] This new critical behavior exists in the whole (C_R, C_L) plane, where also superdiffusion occurs.[7,21] Since $\langle S \rangle$ and $\langle R^2 \rangle$ are both divergent everywhere, σ cannot be defined either.

6. CRITICAL BEHAVIOR OF THE ROTATOR AND THE MIRROR MODEL ON THE TRIANGULAR LATTICE

6.1. The Fully Occupied Lattice

In order to investigate the universality of the trajectory scaling behavior found on the square lattice, we also studied the triangular lattice. Similar to the rotator and mirror models on the square lattice, either fixed rotators or fixed mirrors are randomly placed on the sites of the triangular lattice. The particle can move in six directions along the bonds of the lattice and its velocity is rotated by scatterers over an angle of $\pm 2\pi/3$ upon each collision.[3,7] Since both the mirror model and the rotator model are discussed in this section, in order to avoid confusion, we define C_R^{rotator} and C_L^{rotator} as the concentrations for right rotators and left rotators, respectively, while we define C_R^{mirror} and C_L^{mirror} as the concentrations for right mirrors and left mirrors, respectively. Similarly as before, C represents the total concentration of the scatterers.

For $C=1$ earlier papers have shown[3,7] that the mirror model and the rotator model can be mapped into each other by a global transformation which replaces all the right (left) mirrors on the trajectories by either right (left) rotators or left (right) rotators, respectively, provided $C_R^{\text{rotator}} = C_R^{\text{mirror}}$ and $C_L^{\text{rotator}} = C_L^{\text{mirror}}$. Again it can be shown that the trajectories cannot cross themselves and that all right rotators are either on the outer side or the inner side of the trajectories, depending on the direction in which the particle trajectory closes.

Both the mirror model and the rotator model can now be mapped onto a site percolation rather than a bond percolation problem, as was the case for the rotator and the mirror models on the square lattice. For site percolation on the triangular lattice the critical probability to occupy a lattice site is 1/2, so that the critical point occurs for $C_L^{\text{mirror}} = C_R^{\text{mirror}} = C_L^{\text{rotator}} = C_R^{\text{rotator}} = 1/2$. Here we will only consider the rotator model, since the mirror model can be done in the same fashion. The number of right rotators N_R and the number of left rotators N_L contained in the closed trajectories exhibit the same power-law behavior as on the square lattice [cf. Eq. (4) and Fig. 3],

$$\langle N_R/N - 1/2 \rangle_c = \langle 1/2 - N_L/N \rangle_{cc} \sim N^{-0.57} \tag{32}$$

where $N = N_R + N_L$.

For the triangular lattice the maximum number of times a site on a trajectory can be visited by the moving particle is three. This can be shown by considering again the winding angle W. Upon each collision, W will

either increase or decrease by $2\pi/3$. Therefore, when the particle returns to the same site, $|W|$ will be a multiple of $2\pi/3$. However, there are only three allowed values for $|W|$ on the triangular lattice of the form $2n\pi/3$, where n can be 0, 1, or 2, so that the maximum number of times a site can be visited by the moving particle is indeed three. Accordingly, we define N_1, N_2, and N_3 as the number of sites visited by the particle once, twice and three times, respectively, while S is the length of the trajectory. These quantities satisfy the following two sum rules:

$$N_1 + N_2 + N_3 = N \tag{33}$$

$$N_1 + 2N_2 + 3N_3 = S \tag{34}$$

The scaling behavior of N_1/N, N_2/N, and N_3/N is similar to that found on the square lattice [Eq. (7) and Fig. 4],

$$\langle N_1/N - K_1 \rangle \sim \langle K_2 - N_2/N \rangle \sim \langle K_3 - N_3/N \rangle \sim N^{-0.57} \tag{35}$$

where $K_1 = 0.3197$, $K_2 = 0.4052$, $K_3 = 0.2751$. The sum of K_1, K_2, and K_3 is one, as required by Eq. (33). Although all values of K_i $(i = 1, 2, 3)$ are close to 1/3, they are not equal. The asymptotic scaling behavior for S/N follows from Eqs. (34) and (35) to be

$$\langle S/N - 1.9554 \rangle \sim N^{-0.57} \tag{36}$$

6.2. The Partially Occupied Lattice

For the partially occupied lattice, i.e., $C < 1$, the rotator model and the mirror model can still be mapped into each other by a global transformation. However, neither of the two models can be mapped onto a percolation problem, because the trajectories can cross themselves via empty sites. Nevertheless it was found numerically by Cohen and Wang[7] that for $C < 1$ there exists a linear critical line $C_R = C_L = C/2$, and the trajectory length distribution exponent $\tau = 15/7$ and the fractal dimension $d_f = 7/4$ of the trajectories along this critical line belong to the same universality class as that of site percolation. However, the existence of this single critical line at low concentrations could not be established for concentrations below $C_R = C_L = C/2 = 0.225$, due to the prohibitively long numerical calculations needed.

Since the trajectories can cross themselves, the winding angle W for closed trajectories is no longer restricted to 2π or -2π, so that it is natural

to study the scaling behavior of W. Our numerical results for $C_R = C_L = C/2 = 0.45$ show the relation

$$\langle |W(N)/N| \rangle \sim N^{-0.50} \tag{37}$$

in contrast to the stretched exponential behavior for the rotator model on the partially occupied square lattice, Eq. (9).

For N_R, N_L, and N_E our numerical simulations yield [cf. Eq. (10) and Fig. 6]

$$\langle |N_R/N - C_R| \rangle \sim \langle |N_L/N - C_L| \rangle \sim \langle |N_E/N - C_E| \rangle \sim N^{-0.50} \tag{38}$$

the same as that of the partially occupied square lattice. The exponent 0.50 can be understood in the same way as for the mirror model for $C = 1$.

Using the same kind of argument as we used above for the fully occupied lattice, we can show that the maximum number a site on a trajectory can be visited by the moving particle is three. Unlike for the rotator model on the partially occupied square lattice [cf. Eq. (13)] we find that N_1/N, N_2/N, and N_3/N now follow the same scaling behavior along the critical line as the rotator model on the fully occupied square lattice [cf. Eq. (7)],

$$\langle N_1/N - K_1 \rangle \sim \langle K_2 - N_2/N \rangle \sim \langle K_3 - N_3/N \rangle \sim N^{-0.57} \tag{39}$$

where K_1, K_2, K_3 are functions of the concentration, which sum to 1, while the exponent -0.57 is independent of the concentration. Our numerical simulations also show that K_1 is not a monotonic function of C, while K_2 is an increasing function of C and K_3 is a decreasing function of C. However, all K_i $(i = 1, 2, 3)$ appear to converge to three different constants as C decreases.[15]

7. CRITICAL REGION OF THE ROTATOR AND THE MIRROR MODEL ON THE TRIANGULAR LATTICE

7.1. The Fully Occupied Lattice

Since the rotator model and mirror model are equivalent on the triangular lattice, we only study the rotator model. The procedure is similar as for the square lattice (cf. Section 4).

Our numrical calculations of the scaling function $f(x)$ were carried out at $C_R = 0.47$, 0.48, and 0.49, respectively. The scaling functions for

these three concentrations collapsed onto a single curve, which could be fitted again to a double Gaussian [cf. Eq. (23)],

$$f(x) = 0.94e^{-1.80(x+0.96)^2} + 0.94e^{-1.80(x-0.96)^2} \tag{40}$$

where for each C_R more than 60 points were computed and the curve comprises therefore more than 180 points. Equations (23) and (40) only differ in the constants occurring in the equations. When $x \gg 1$, $f(x) \sim e^{-x^2}$, so $n_S \sim e^{-S^{6/7}}$, the same as for the square lattice.

The calculation of the scaling function $h(x)$ is also similar to that for the square lattice. We again found numerically that $f(x)\,h(x)$ is proportional to $f(x)$ [cf. Eq. (26)],

$$f(x)\,h(x) = 0.28e^{-1.80(x+0.96)^2} + 0.28e^{-1.80(x-0.96)^2} \tag{41}$$

so that $h(x)$ is a constant, $0.28/0.94 = 0.30$.

The average trajectory size diverges as one approaches criticality with an exponent γ, $\langle S \rangle \sim (C_R - C_{R_c})^{-\gamma}$. Our numrical simulations show that $\gamma = 2.0 \pm 0.01$, in good agreement with the exact result, $\gamma = 2$. The mean square displacement of the particle trajectories diverges with an exponent ρ, $\langle R^2 \rangle \sim (C_R - C_{R_c})^{-\rho}$; the value of ρ obtained from our numerical simulations is 2.33 ± 0.01, also in good agreement with the exact result $\gamma = 7/3$ (cf. Figs. 12 and 13).

Using the histogram method, we computed the scaling functions also from the standard data obtained at the concentration $C_R = 0.51$ for the other concentrations $C_R = 0.52$, 0.53, 0.54, 0.55. All the scaling functions $f(x)$ fall then on the same curve given by Eq. (40), showing that this method is consistent with the first one.

7.2 The Partially Occupied Lattice

For $C < 1$ the rotator model and the mirror model can be still mapped onto each other. However, neither model can be mapped onto a percolation problem now, Here we only consider the rotator model. It was found before that there is only one critical line $C_R = C_L$ with critical exponents $\tau = 15/7$ and $d_f = 7/4$, the same as those at the critical point, $C_{R_c} = C_{L_c} = 1/2$.[3,7]

To study the critical behavior near criticality, we first need to choose the direction in which we approach criticality. The most obvious choice is the direction perpendicular to the critical line. Although the rotator model cannot be mapped onto a percolation problem, we found nevertheless that if we choose $\sigma = 3/7$, the scaling functions computed at different C_R collapse very well onto a single curve. This suggests that randomly distributed empty sites

on the lattice are irrelevant for the critical behavior. The scaling functions were computed in the critical region near $C_{R_c} = C_{L_c} = 0.425$ at three different C_R, $C_R = C_{R_c} + 0.01$, $C_R = C_{R_c} + 0.015$, and $C_R = C_{R_c} + 0.02$, along the line $C = 0.85$. We found that these scaling functions could be fitted to a double Gaussian [cf. Eq. (23) and Fig. 10],

$$f(x) = 1.05e^{-1.18(x+1.19)^2} + 1.05e^{-1.18(x-1.19)^2} \tag{42}$$

where we computed 80 points for each C_R, leading to 240 points on the curve.

The product of $f(x)\,h(x)$ is again found to be proportional to $f(x)$ [cf. Eq. (6) and Fig. 11],

$$f(x)\,h(x) = 0.30e^{-1.18(x+1.19)^2} + 0.30e^{-1.18(x-1.19)^2} \tag{43}$$

so that $h(x) = 0.30/1.05 = 0.28$.[15] Comparing Eqs. (40) and (43), respectively, one can see that all three constants contained in $f(x)$ and $h(x)$ are concentration dependent.

To investigate whether the critical exponent σ has the same value along the critical line, we also computed $\langle S \rangle$ and $\langle R^2 \rangle$ in the critical region around $C_{R_c} = C_{L_c} = 0.45$ and $C_{R_c} = C_{L_c} = 0.4$, respectively. In both cases we found from our numerical simulations that the exponents $\gamma = 2.00 \pm 0.02$ and $\rho = 2.33 \pm 0.02$ are very close to their values at $C_{R_c} = C_{L_c} = 0.5$: 2 and 7/3, respectively, suggesting that the critical behavior along the critical line $C_R = C_L$ belongs indeed to the same universality class (cf. Section 4).

8. CONCLUSION

In this paper we have given a more detailed numerical analysis than before of the nature of the trajectories generated in a Lorentz lattice gas cellular automaton on both the square lattice and the triangular lattice at and near criticality.

Our study has shown that the "structural" properties of these trajectories are highly nontrivial and yield especially some new scaling behavior related to the scaling function exponent σ, in addition to that associated with the critical exponents τ and d_f found before. The results are summarized in Tables I–IV.

Our study raises many questions, among which we note the following.

1. It is unclear why the critical exponents associated with percolation clusters also have significance for the dynamics of particle trajectories on a partially occupied lattice, where no mapping exists between the two.

Table I. Critical Behavior for $C=1$

Square lattice		Triangular lattice
Rotator	Mirror	Rotator = Mirror
$\langle N_R/N-1/2\rangle_c$ $=\langle N_L/N-1/2\rangle_{cc}\sim N^{-0.57}$	$\langle \lvert M_R/N-C_R\rvert\rangle$ $=\langle \lvert M_L/N-C_L\rvert\rangle\sim N^{-0.50}$	$\langle N_R/N-1/2\rangle_c$ $=\langle N_L/N-1/2\rangle_{cc}$ $\sim N^{-0.57}$
$\langle N_1/N-1/2\rangle$ $=\langle 1/2-N_2/N\rangle\sim N^{-0.57}$	$\langle N_1/N-a(C_R)\rangle$ $=\langle b(C_R)-N_2/N\rangle=N^{-0.57}$	$\langle N_1/N-0.3197\rangle$ $\sim\langle 0.4052-N_2/N\rangle$ $\sim\langle 0.2751-N_3/N\rangle$ $\sim N^{-0.57}$
$\langle S/N-3/2\rangle\sim N^{-0.57}$	$\langle S/N-1-b(C_R)\rangle\sim N^{-0.57}$	$\langle S/N-1.9554\rangle$ $\sim N^{-0.57}$

2. For $C=1$, why are the asymptotic values of N_R and N_L as well as of N_1 and N_2 on the fully occupied square lattice equal to $N/2$? Why, for the fully occupied triangular lattice, are N_R and N_L also equal to $N/2$, while N_1, N_2, and N_3 approach different asymptotic values K_1, K_2, and K_3, respectively?

3. Although we have given an argument why the exponents describing the fluctuations of N_R/N along the critical line $C=1$ for the mirror

Table II. Critical Behavior for $C=0.9$

Square lattice		Triangular lattice
Rotator	Mirror	Rotator = Mirror
$\langle \lvert W/N-(C_R-C_L)\rvert\rangle\sim 2^{-2.85^{0.18}}$	superdiffusion ($\tau=1$, $d_f=2$)	$\langle \lvert W/N\rvert\rangle\sim N^{-0.50}$
$\langle \lvert N_R/N-C_R\rvert\rangle$ $=\langle \lvert N_L/N-C_L\rvert\rangle$ $\sim\langle \lvert N_E/N-C_E\rvert\rangle\sim N^{-0.50}$		$\langle \lvert N_R/N-C_R\rvert\rangle$ $=\langle \lvert N_L/N-C_L\rvert\rangle$ $\sim\langle \lvert N_E/N-C_E\rvert\rangle\sim N^{-0.50}$
$\langle N_1/N-0.2671\rangle$ $\sim\langle N_2/N-0.3047\rangle$ $\sim\langle 0.2223-N_3/N\rangle$ $\sim\langle 0.2059-N_4/N\rangle\sim N^{-0.39}$		$\langle N_1/N-0.3308\rangle$ $\sim\langle 0.3669-N_2/N\rangle$ $\sim\langle 0.3023-N_3/N\rangle\sim N^{-0.57}$
$\langle S/N-2.3670\rangle\sim N^{-0.39}$		$\langle S/N-1.9715\rangle\sim N^{-0.57}$

Table III. Critical Behavior for $C = 0.8$

Square lattice		Triangular lattice
Rotator	Mirror	Rotator = Mirror
$\langle \lvert W/N - (C_R - C_L) \rvert \rangle \sim 2^{-1.45^{0.18}}$	superdiffusion ($\tau = 1, d_f = 2$)	$\langle \lvert W/N \rvert \rangle \sim N^{-0.50}$
$\langle \lvert N_R/N - C_R \rvert \rangle$ $= \langle \lvert N_L/N - C_L \rvert \rangle$ $\sim \langle \lvert N_E/N - C_E \rvert \rangle \sim N^{-0.50}$		$\langle \lvert N_R/N - C_R \rvert \rangle$ $= \langle \lvert N_L/N - C_L \rvert \rangle$ $\sim \langle \lvert N_E/N - C_E \rvert \rangle \sim N^{-0.50}$
$\langle N_1/N - 0.2680 \rangle$ $\sim \langle N_2/N - 0.2760 \rangle$ $\sim \langle 0.2365 - N_3/N \rangle$ $\sim \langle 0.2195 - N_4/N \rangle \sim N^{-0.39}$		$\langle N_1/N - 0.3356 \rangle$ $\sim \langle 0.3391 - N_2/N \rangle$ $\sim \langle 0.3254 - N_3/N \rangle \sim N^{-0.57}$
$\langle S/N - 2.4075 \rangle \sim N^{-0.39}$		$\langle S/N - 1.990 \rangle \sim N^{-0.57}$

model are all equal to 0.50, the more fundamental exponent 0.57 remains elusive. We conjecture that the exact value is $1 - \sigma = 4/7$, but it is not clear how to obtain this from theory.

4. We find that the N_i/N approach their asymptotic values K_i with a power law $N^{-0.57}$ in all cases, except for the rotator model on the partially occupied square lattice, where the exponent has a significantly different value, 0.39. We also found that σ appears to have the same value 3/7 in all cases, except again for the rotator model on the partially occupied square lattice, where we found a value $\sigma' = 1.6 \pm 0.3$. Thus the scaling behavior of the N_i/N and the exponent σ appear to be related to each other, but it is unclear in what way.

5. Why does the winding angle W of the rotator model on the partially occupied square lattice exhibit a stretched-exponential-law behavior, while it exhibits a simple power-law behavior on the partially occupied triangular lattice?

6. For the rotator model on the partially occupied square lattice the new scaling function $f'(x)$, corresponding to the exponent $\sigma' = 1.6 \pm 0.3$, appears to be an exponential function, not the double Gaussian as for $C = 1$; the origin of this exceptional critical behavior is unclear to us. However, for the partially occupied triangular lattice we found a scaling function $f(x)$ still described by a double Gaussian and a σ very close to 3/7, which also obtains for $C = 1$. This suggests that for this lattice the

Table IV. Scaling Functions and Critical Exponents[a]

		Lattice			
		Square		Triangular	
		$C=1$	$C<1$	$C=1$	$C<1$
Scaling functions					
$f(x)$ (double Gaussian)	A_1	1.03	—	0.94	1.05
	α_1	2.25	—	1.80	1.18
	a_1	0.86	—	0.96	1.19 ($C=0.85$)
$h(x)$ (constant)		0.38		0.30	0.28
$f'(x)$ (exponential)	A_1'		0.475		
	α_1'		1.65×10^{-8}		
	a_1'		0		
$h'(x)$ (constant)			0.24		
Exponents					
τ		15/7	15/7	15/7	15/7
d_f		7/4	7/4	7/4	7/4
$\sigma(\sigma')$		3/7	1.6	3/7	3/7
$\gamma(\gamma')$		2	0.54	2	2
$\rho(\rho')$		7/3	0.63	7/3	7/3

[a] Scaling functions and critical exponents obtained for closed trajectories on the square and triangular lattices. $f(x)=A_1\exp[-\alpha_1(x-a_1)^2]+A_1\exp[-\alpha_1(x+a_1)^2]$ and $f'(x)=A_1'\exp[-\alpha_1'(x-a_1')]$. The critical exponents for $C=1$ are known exactly, those for $C<1$ only numerically. The square lattice for $C<1$ behaves exceptionally if the critical point $C_{R_c}=C_{L_c}=1/2$ is approached along the line $C_R=C_L$ rather than along the line $C=1$; the primed quantities refer to this case.

critical behavior in the direction perpendicular to the critical line $C_R=C_L$ is in one univerality class.

7. The scaling function $h(x)$ appears to behave like a constant in all cases, indicating that there are no noticeable corrections to the universal fractal dimension $d_f=7/4$. This simply means that the gyration radius of the extended trajectories is independent of the degree of occupation of the lattice by scatterers and only trivially dependent on the nature of the lattice.

8. We have studied the scaling behavior of extended particle trajectories as their sizes approach infinity *at* criticality. For example, we have obtained for the rotator model on the fully occupied square lattice that $\langle S/N-3/2\rangle\sim N^{-0.57}$, where the exponent is very close to $1-\sigma=4/7=0.571$, with σ characterizing the trajectory size distribution in the critical region *near* criticality.

We surmise that this may not be a coincidence and conjecture that there is a possible relation between the scaling behavior of extended closed trajectories *at* criticality and in the critical region *near* criticality. If so, the question arises whether also other exponents such as γ and ρ could be determined from the scaling behavior at criticality, rather than, as we have done here, in the critical region. This behavior is also reminiscent of, although quite different from, the fluctuation-dissipation theorem, for here it concerns a connection between the behavior of a system at and near a critical point in equilibrium, rather than the behavior of a system at and near equilibrium.[25]

ACKNOWLEDGMENTS

The authors are grateful to J. Machta, B. Nienhuis, F. Wang, and R. Ziff for helpful comments. This work was supported under grant DE-FG02-88ER13847 of the Department of Energy.

REFERENCES

1. Th. W. Ruijgrok and E. G. D. Cohen, *Phys. Lett. A* **133**:415 (1988).
2. X. P. Kong and E. G. D. Cohen, *Phys. Rev. B* **40**:4838 (1989).
3. X. P. Kong and E. G. D. Cohen, *J. Stat. Phys.* **62**:737 (1991).
4. R. M. Ziff, X. P. Kong, and E. G. D. Cohen, *Phys. Rev. A* **44**:2410 (1991).
5. E. G. D. Cohen, New types of diffusion in lattice gas cellular automata, in *Microscopic Simulations of Complex Hydrodynamic Phenomena*, M. Mareèchal and B. L. Holian, eds. (Plenum Press, New York, 1992), p. 137.
6. H. F. Meng and E. G. D. Cohen, *Phys. Rev. E* **50**:2482 (1994).
7. E. G. D. Cohen and F. Wang, *J. Stat. Phys.* **81**:445 (1995).
8. F. Wang and E. G. D. Cohen, *J. Stat. Phys.* **81**:467 (1995).
9. E. G. D. Cohen and F. Wang, *Physica A* **219**:56 (1995).
10. E. G. D. Cohen and F. Wang, *Fields Inst. Commun.* **6**:43 (1996).
11. F. Wang and E. G. D. Cohen, *J. Stat. Phys.* **84**:233 (1996).
12. D. Stauffer and A. Aharony, *Introduction to Percolation Theory* (Taylor and Francis, London, 1992).
13. R. M. Ziff, *Phys. Rev. Lett.* **56**:545 (1986).
14. R. M. Ziff, P. T. Cumming, and G. Stell, *J. Phys. A* **17**:3009 (1984).
15. M.-S. Cao and E. G. D. Cohen, cond-mat@xxx.lanl.gov #9608159, #9608160 (1996).
16. P. Grassberger, *J. Phys. A* **19**:2675 (1986).
17. R. M. Ziff, Private communication.
18. M. Ortuño, J. Ruiz, and M. F. Gunn, *J. Stat. Phys.* **65**:453 (1991).
19. L. A. Bunimovich and S. E. Troubetzkoy, *J. Stat. Phys.* **67**:289 (1992); **74**:1 (1994).
20. R. M. Bradley, *Phys. Rev. B* **41**:914 (1989).
21. A. L. Owczarek and T. Prellberg, *J. Stat. Phys.* **79**:951 (1995).
22. J. D. Catalá, J. Ruiz, and M. Ortuño, *J. Phys. B* **90**:369 (1993).
23. P. L. Leath, *Phys. Rev. Lett.* **36**:921 (1976); *Phys. Rev. B* **14**:5046 (1976).
24. A. M. Ferrenberg and R. H. Swendsen, *Phys. Rev. Lett.* **61**:2635 (1988).
25. J. P. Hansen and I. R. McDonald, *Theory of Simple Liquids* (Academic Press, London, 1986), p. 106.